LA-UR-02-2212
Approved for public release; distribution is unlimited.

Title: **Statistical Comparison between Experiments and Numerical Simulations of Shock-Accelerated Gas Cylinders**

Author(s): William J. Rider, James R. Kamm, Cindy A. Zoldi, and Christopher D. Tomkins

Submitted to: **WCCM V** Fifth World Congress on Computational Mechanics, July 7–12, 2002, Vienna, Austria

http://lib-www.lanl.gov/cgi-bin/getfile?00818827.pdf

WCCM V
Fifth World Congress on
Computational Mechanics
July 7–12, 2002, Vienna, Austria
Eds.: H.A. Mang, F.G. Rammerstorfer,
J. Eberhardsteiner

Statistical Comparison between Experiments and Numerical Simulations of Shock-Accelerated Gas Cylinders

William J. Rider, James R. Kamm*, Cindy A. Zoldi, and Christopher D. Tomkins

Los Alamos National Laboratory
MS D413, Los Alamos, NM 87545, USA
e-mail: kammj@lanl.gov

Key words: Richtmyer-Meshkov instability, high resolution numerical methods, validation, fractal spectrum, wavelet analysis

Abstract
We present detailed spatial analysis comparing experimental data and numerical simulation results for Richtmyer-Meshkov instability experiments of Prestridge et al. [11] and Tomkins et al. [19]. These experiments consist, respectively, of one and two diffuse cylinders of sulphur hexaflouride (SF_6) impulsively accelerated by a Mach 1.2 shockwave in air. The subsequent fluid evolution and mixing is driven by the deposition of baroclinic vorticity at the interface between the two fluids. Numerical simulations of these experiments are performed with three different versions of high resolution finite volume Godunov methods, including a new weighted adaptive Runge-Kutta (WARK) scheme [15]. We quantify the nature of the mixing using using integral measures as well as fractal analysis and continuous wavelet transforms. Our investigation of the gas cylinder configurations follows the path of our earlier studies of the geometrically and dynamically more complex gas "curtain" experiment [13, 14]. In those studies, we found significant discrepancies in the details of the experimentally measured mixing and the details of the numerical simulations. Here we evaluate the effects of these hydrodynamic integration techniques on the diffuse gas cylinder simulations, which we quantitatively compare with experimental data.

1 Introduction

We examine the detailed structure of experiments and simulations involving shock-driven mixing initiated by the Richtmyer-Meshkov (RM) instability [3]. The experiments consist of a heavy gas (SF_6) that is introduced into a light gas (air) by a configurable nozzle and is impulsively accelerated by a planar Mach 1.2 shock wave; see [16, 17] for details. In previous work [13, 14], we examined the shock-driven evolution of a varicose-profile, thin gas layer (a gas "curtain"); the present work examines shock interactions with one or two diffuse gas cylinders. The fluid mixing in these experiments is driven by the deposition of baroclinic vorticity at the interface between the two fluids, producing the RM instability. Multi-exposure flow visualization is obtained with laser-sheet illumination, providing several snapshots of the SF_6 volume fraction.

Our computational simulations were performed with different codes and algorithms, to examine the effects of the numerics on the characteristics of the computed mixing flow. These results do not include explicitly modeled viscous terms; a more limited set of complementary simulations of this configuration with equations that *do* contain viscous terms indicates no substantial difference in the computed results. The RAGE code [1] employs a high resolution Godunov method that is implemented in a dimensionally split Lagrange-remap (SLR) fashion with a linearized two-shock Riemann solver. This code has genuine multimaterial capability, with local thermal, pressure, and momentum equilibrium enforced. This code also has an adaptive mesh refinement (AMR) feature, which was activated in the calculations. The CUERVO code is principally used to investigate advanced numerical integration techniques and uses a Godunov method with a simple multimaterial treatment introduced by Bell et al. [2]. This code uses unsplit differencing (both spatial and temporal) together with an adaptive quadratic two-shock Riemann solver [12] in either a standard high resolution unsplit direct Eulerian (UDE) method or with a new weighted adaptive Runge-Kutta (WARK) scheme [15].

We compare the experimental images with the computed results both qualitatively and quantitatively. Given the sensitive dependence on the initial conditions for these flows, one cannot perform pointwise comparison of the flowfields. Therefore, we examine the data and results with more general methods. The quantitative analysis techniques we consider include fractal analysis and continuous wavelet transforms. With these methods we seek to quantify flow structures over a range of length scales. We find that some simulation results correspond quantitatively to experiments at certain length scales, while others deviate significantly. The details of the numerical integration appear to play a significant role in this variation.

This paper is structured as follows. The experimental configuration is discussed in further detail in §2. A brief description of the simulation codes is provided in §3. The analysis techniques are briefly described in §4. Results are provided in §5, followed by a summary in §6.

2 The Shock Tube Richtmyer-Meshkov Experiment

Richtmyer-Meshkov experiments were conducted at the Los Alamos facility (Fig. 1) by Prestridge et al. [11] and Tomkins et al. [19]. We describe them briefly and focus on aspects that are relevant to our current discussion. The experimental apparatus is a 5.5 m shock tube with a 7.5 cm $\times$ 7.5 cm square test section. The driver section is pressurized before the shot, and the rupturing of a polypropylene diaphragm produces a Mach 1.2 planar shock. In the test section, heavy SF_6 gas is injected vertically through a nozzle in the top, and removed by suction through an exhaust plenum at the bottom. The nozzle shape imposes a specified shape on the cross section of the SF_6, which has a downward velocity of ~ 10 cm/s.

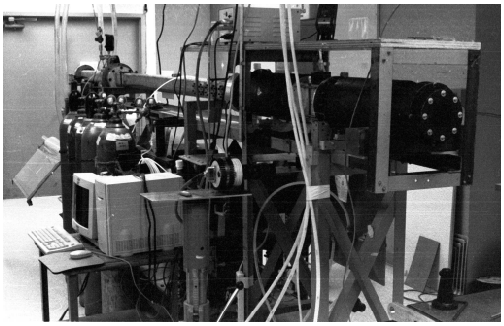

Figure 1: Photograph of the shock tube experimental facility.

The experiments of interest used single or double column(s) of SF_6. In the latter case, Tomkins et al. [19] consider several values of the inter-cylinder spacing S for fixed cylinder diameter D; we examine the three cases $S/D = 1.2$, 1.5, and 2.0. The evolution of the subsequent flow, which is illuminated by a horizontal laser light sheet, remains approximately two-dimensional for the span of the experiment (although it eventually transitions to a fully three-dimensional flow) and exhibits substantial shot-to-shot repeatability. A tracer material consisting of glycol fog (with characteristic droplet dimension of 0.5 μm) is added to the SF_6 to greatly enhance the dynamic range of the images, which are captured by CCD camera. A detailed discussion of the experimental apparatus, including a discussion of the flow tracking characteristics of the glycol fog and experimental error analysis, is given by Rightley et al. [17] Images, which are obtained at 50, 190, 330, 470, 610, and 750 μs after shock impact with the cylinder(s), have a pixel resolution of ~ 0.01 cm $\times$ 0.01 cm. The image intensity corresponds to the volume fraction of SF_6, since the signal registered at the CCD is proportional to the number of scatterers in each pixel volume.

The imaged flows are transitional (i.e., not fully turbulent) in nature, with an integral scale circulation-based Reynolds number of $\sim 10^4$–10^5, a measured Taylor microscale Reynolds number of ~ 1500, and a Taylor microscale length of ~ 1.5 mm. Table 1 provides the initial gas properties used in the simulations.

Table 1: Physical properties of the gases used in the simulations.

Material	ρ (g cm^{-3})	p (dyn cm^{-2})	γ	C_v (erg °K g^{-1})	η (dyn s cm^{-2})
Pre-Shock Air	1.00×10^{-3}	0.80×10^{6}	1.40	6.89×10^{6}	1.8×10^{-4}
Post-Shock Air	1.34×10^{-3}	1.21×10^{6}	1.40	6.89×10^{6}	1.8×10^{-4}
Pre-Shock SF_6	5.00×10^{-3}	0.80×10^{6}	1.09	5.52×10^{6}	1.5×10^{-4}

3 Numerical Simulations

Several aspects of the numerical simulations greatly influence the computed results. All computations were run in a frame of reference in which the post-shock SF_6 structure is approximately stationary; the imposed translational velocity counteracts the shock- and vorticity-induced velocity of the cylinder(s), thereby decreasing the horizontal motion of the SF_6 structure through the computational mesh.

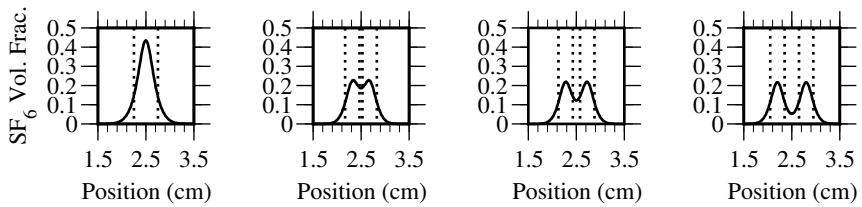

Figure 2: Initial volume fractions for the simulations: from left to right, the single cylinder and the $S/D = 1.2$, 1.5, and 2.0 double cylinders.

3.1 Initial Conditions

The initial conditions for the SF_6 are extremely important because the first shock-cylinder interaction determines much of baroclinic vorticity deposition, which greatly influences the subsequent evolution. Our previous gas curtain study [13, 14] used experimental data to initialize the simulations; however, in this work we use idealized initial data. Efforts are presently underway to obtain high resolution initial condition images to be used in computational initialization. For this study, we operate on initially Gaussian regions of SF_6 (full-width at half-maximum diameter D of 0.5 cm and 0.3 cm for the single and double cylinders, respectively) with a numerical isotropic diffusion operator, using an empirically chosen number of diffusion iterations so that resulting volume fraction profiles correspond to initial experimental measurements. Figure 2 contains plots of the SF_6 centerline volume fractions used as the initial conditions for each simulation.

3.2 Simulation Codes

Computations were done with two hydrocodes: RAGE, an adaptive grid Godunov method [1], and CUERVO, a Godunov code for investigating advanced hydrodynamics algorithms [12]. Both codes nominally solve the multimaterial Euler equations of compressible flow. We performed simulations with two different codes to quantify the effect of the different solution algorithms in these codes on the large-scale (integral) and small-scale (statistical) characteristics of the simulated shock-induced mixing flow. Neither of these codes includes explicitly modeled viscous terms; however, a limited number of complementary simulations with equations containing viscous terms indicates no substantial difference in the computed results.

RAGE is a high resolution Godunov code in which the hydro algorithm is operator split and implemented in a Lagrange-remap fashion with a linearized two-shock Riemann solver. The code has genuine multimaterial capability with the fluids forced to be in local thermal, pressure, and momentum equilibrium. RAGE contains adaptive mesh refinement (AMR) technology, which we employed to mesh the entire shock tube, with reflective boundaries at edges of the computational domain. Additionally, RAGE is capable of effectively utilizing the most modern computing resources available.

CUERVO is principally used to investigate advanced numerical integration techniques. CUERVO has unsplit differencing (both spatial and temporal), a basic multimaterial treatment [2], and an adaptive quadratic two-shock Riemann solver [12] with either a standard high resolution unsplit direct Eulerian method or the new weighted adaptive Runge-Kutta scheme [15]. In the present calculations, outflow boundary conditions are imposed at the edges of the computational mesh, which is comprised of a 5 cm $\times$ 5 cm domain.

3.3 New Hydrodynamics Algorithm

Our earlier gas curtain comparisons suggested that the hydrodynamics algorithm plays a significant role in the computed dynamics. The standard numerical methods did not faithfully reproduce the details of the experimental gas curtain data, which led us to careful consideration of the basic hydrodynamics algorithm. That investigation, together with numerical tests, suggested that the high-order terms associated with acoustic wave propagation may have affected our gas curtain simulations. Those calculations also exhibited a surprising degree of temporal oscillations; such behavior is related to sound waves interacting with density variations in the flow. Further examination indicated that such features are often not detected by the spatial differencing, prompting us to consider *temporal* adaptation of the algorithm.

Standard differencing methods are typically adaptive in space, with the time differencing remaining identical for all cells (and usually all time steps). That is, adaptivity—by which we mean differencing algorithm adaptivity, *not* mesh adaptivity—is implemented solely through the spatial differencing operator. Instead, we emply two independent methods to estimate the time advancement and then nonlinearly merge these results using limiting techniques borrowed from spatial differencing methods. This approach is a *de facto* acknowledgement that the temporal field is varying in a way that is not reflected in the spatial profiles. In a sense, the computed flow field is not evolving in a manner consistent with hyperbolic self-similarity, so that time and space differences may not be freely exchanged.

The weighted adaptive Runge-Kutta method (WARK) scheme [15] uses a nonlinear combination of the usual stages of the Runge-Kutta method as follows. A linear multistep method (Adams-Bashforth) and a forward-in-time technique (Lax-Wendroff style) are *both* used to advance the variables. Where the solution varies smoothly in time, i.e., if these two results agree to some chosen accuracy, the high accuracy scheme result will be recovered. Where the solution varies greatly, i.e., if the two results are sufficiently different in magnitude or vary in sign, then the time differencing is modified by weights that are chosen to bias the solution in favor of the smoother time variation. This nonlinear combination must be computed separately on the fluxes so that the resultant method remains in conservation form. The effect of the temporal adaptation is to make the time differencing a nonlinear, convex combination of the two methods based on the smoothness of each time derivative estimate.

4 Analysis Techniques

Since pointwise comparison of the evolving unstable flow is problematic, we employ statistical methods by which to gauge the sub-integral scale behavior. Specifically, we measure the local fractal dimension and the contiuous wavelet energy spectrum, by which we can *quantitatively* compare, over some range of length scales, experimental observations and computational results. See [9] for further details.

Fractal analysis has been used extensively to characterize, both theoretically and experimentally, turbulent fluid phenomena [18]. We consider the variation method [5] for computing the fractal dimension of a surface. For a given scale ε, one calculates the upper and lower envelopes of the data in local ε-neighborhoods. The ε-variation, computed as mean of the difference between these surfaces, is then used to estimate the overall fractal dimension. The algorithm for this calculation is both more efficient than that for the conventional fractal box counting approach [7] and less complicated to implement. From these results we infer the *local* fractal dimension (akin to the "coverage dimension" of [4]), which is the scaling exponent between each pair of variation-dimension/length-scales data. Although numerical approximations to the fractal dimension suffer from a number of shortcomings [8], such considerations

do not prevent fractal analysis from providing a useful measure with which to *quantitatively* compare experimental data or numerical results that contain complex structure.

The continuous wavelet transform (CWT) [6] is a spectral technique in which a given function or data set is projected onto dilated and translated versions of a basis function, known as the "mother wavelet". The CWT is basically a generalized convolution between the function of interest and a scaled and translated version of the mother wavelet. The CWT has many applications in data analysis [10], including the quantification of turbulent flow data [6, 20]. Due to the required nature of the mother wavelet, the CWT characterizes *local* behavior, unlike the Fourier transform, which quantifies *global* (or *periodic*) characteristics. The mother wavelet we consider is the isotropic Marr or "Mexican hat" wavelet given by $\psi(x,y) = (2-r^2)\exp(-r^2/2)/\sqrt{2\pi}$, where $r^2 \equiv x^2 + y^2$. The *wavelet energy spectrum* [6] can be obtained in terms of the CWT by integrating over translation space, resulting in a scale-dependent measure by which experiments and simulations can be *quantitatively* compared.

5 Results

We focus our analysis on the final experimental volume fraction image, at 750 μs after shock-SF_6 contact, to examine the maximum effect of the nonlinear flow evolution. Calculations were run on meshes with $\Delta x = 0.02$ and 0.01 with all schemes and, additionally, at $\Delta x = 0.005$ for the SLR scheme. The SLR calculations have an overall asymptotic convergence rate of approximately unity.

5.1 The Single Cylinder

Results for the single cylinder volume fraction images, local D_f, and CWT spectra are shown in Figure 3. The local D_f values of the simulations are all comparable except at the largest scales, where the SLR values increase, albeit in a manner different from the experiment. Relatively large values of D_f at large scales were also seen in our earlier gas curtain study. All simulations overestimate the CWT energy at smaller scales, but the UDE and WARK results most closely approximate the experiment over the largest range of scales. Integral scale measures, given in Table 2, also show that the UDE and WARK results most nearly approximate the experiment in these dimensions.

5.2 The Double Cylinder

Results for the volume fraction images, local D_f, and CWT spectra for the three configurations are shown in Figure 4, 5, and 6, respectively. The $S/D = 1.2$ configuration shows the tightest coupling of

Table 2: Integral scale measures of the cylinders at $t = 750$ μs.

	Height (cm)				Width (cm)				Aspect Ratio			
Geometry	Exp.	SLR	UDE	ARK	Exp.	SLR	UDE	ARK	Exp.	SLR	UDE	ARK
Single Cyl.	1.60	1.24	1.51	1.52	1.37	0.93	1.30	1.30	1.17	1.33	1.16	1.17
$S/D = 1.2$	1.28	1.48	1.76	1.76	0.87	0.72	1.01	1.02	1.46	2.06	1.74	1.73
$S/D = 1.5$	1.72	1.64	2.13	2.14	0.76	0.72	0.92	0.92	2.26	2.28	2.32	2.33
$S/D = 2.0$	1.77	1.66	2.30	2.30	0.72	0.69	0.92	0.93	2.45	2.41	2.50	2.47

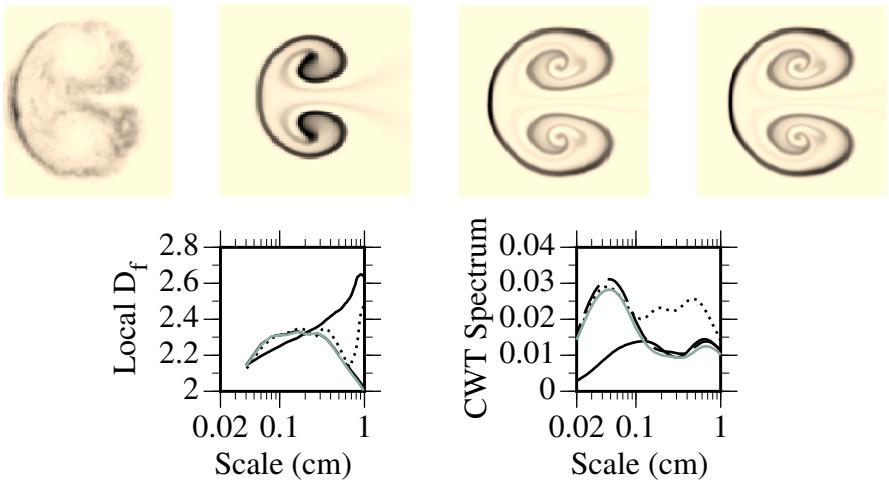

Figure 3: Top row: SF_6 volume fraction images of the single cylinder at $t = 750$ μs post-shock for, from left to right, the experiment (solid), SLR method with $\Delta x = 0.01$ cm (dotted), UDE method on the same grid (grey), and WARK method on the same grid (dashed). Bottom row: corresponding plots of local D_f (left) and CWT spectrum (right) vs. scale.

the vortical structures, due to the diffuse initial condition (see Fig. 2); the final state displays structure evocative of the single cylinder case (cf. Fig. 3). The cases with greater initial separation, Figs. 5 and 6, develop "mushroom caps", like those in ideal RM instability, which rotate with the induced vorticity.

In all cases, the SLR methods gives less roll-up in the mushroom caps and a more pronounced "bridge" between these structures. For the SLR method, this may be related to the minmod limiter used. Overall, the gross morphology of the UDE and WARK results (e.g., the roll-up) qualitatively approximates the experiment more closely than SLR. The integral scale measures, given in Table 2, are the dimensions of the box that bounds the entire structure; in these measures, the more compact SLR structures most closely match the experimental data overall.

Examination of the statistical measures reveals differences primarily between the SLR and UDE/WARK codes. In each case, the local D_f at smaller scales is comparable among the simulations; at intermediate scales, the UDE and WARK results more closely match the data, especially in the $S/D = 1.5$ and 2.0 cases. Only at the largest scales in the $S/D = 1.2$ and 2.0 does the behavior of the SLR results better approximate the experiment.

The CWT spectra of the simulations are largely comparable at the smallest scales, again overshooting the experimental values. The UDE and WARK values are virtually identical and most closely approximate the experiment overall. Only in the $S/D = 1.2$ case does the SLR code give slightly better CWT results.

6 Summary

We have examined the gas curtain Richtmyer-Meshkov experiments of Prestridge et al. [11] and Tomkins et al. [19] together with idealized numerical simulations of these experiments using different hydrodynamics algorithms. All simulations exhibit qualitatively similar behavior for the single cylinder, while the double cylinder appears to be a more sensitive configuration. Although the new WARK method gave superior results for gas curtain simulations initialized with an experimental image, this new adaptive time

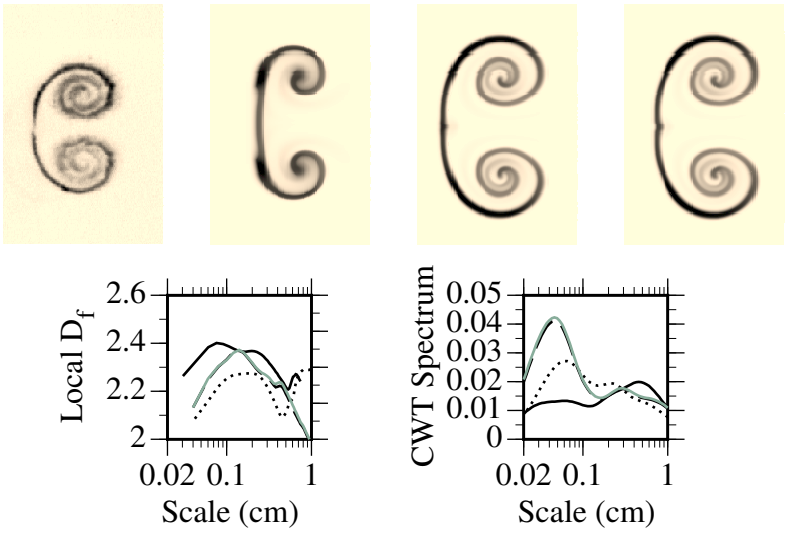

Figure 4: Top row: SF_6 volume fraction images of the $S/D = 1.2$ double cylinder at $t = 750$ μs post-shock for, from left to right, the experiment (solid), SLR with $\Delta x = 0.01$ cm (dotted), UDE on the same grid (grey), and WARK on the same grid (dashed). Bottom row: corresponding plots of local D_f (left) and CWT spectrum (right) vs. scale.

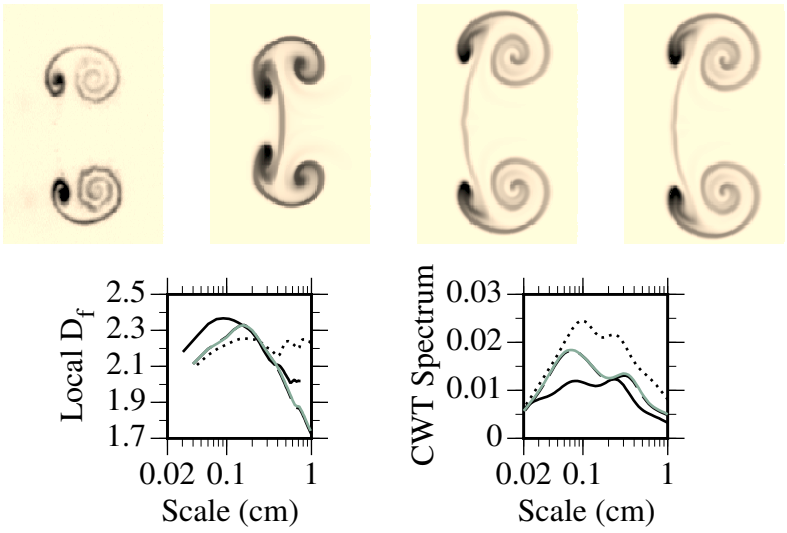

Figure 5: Top row: SF_6 volume fraction images of the $S/D = 1.5$ double cylinder at $t = 750$ μs post-shock for, from left to right, the experiment (solid), SLR with $\Delta x = 0.01$ cm (dotted), UDE on the same grid (grey), and WARK on the same grid (dashed). Bottom row: corresponding plots of local D_f (left) and CWT spectrum (right) vs. scale.

differencing algorithm is virtually identical, in fractal and wavelet spectra, to a standard UDE scheme in these simulations of shocked gas cylinders with diffused idealized initial conditions. Consistent with this result, we speculate that WARK and UDE results may differ at later (scaled) times, when nonlinearities in both the flow and the algorithms would be more fully developed. Examination of experimental particle image velocimetry data will help us to better understand the differences between experiments and simulations, as will quantification of ensembles of experimental and simulation realizations.

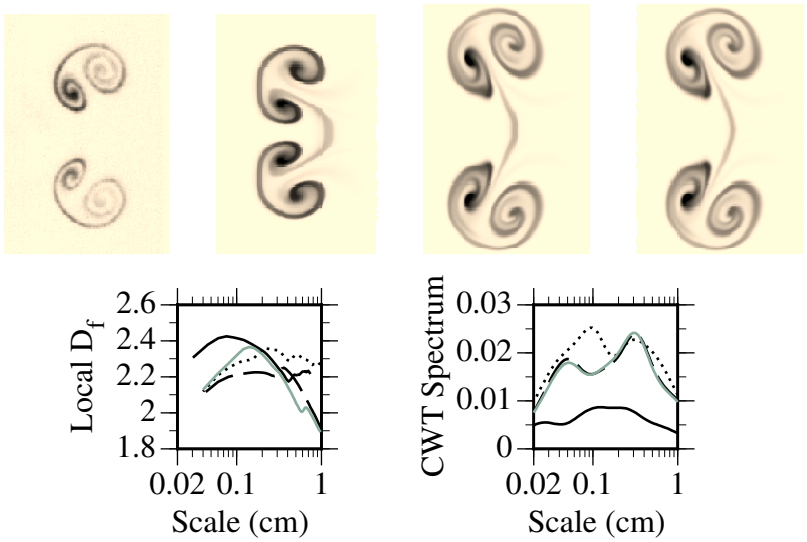

Figure 6: Top row: SF_6 volume fraction images of the $S/D = 2.0$ double cylinder at $t = 750$ μs post-shock for, from left to right, the experiment (solid), SLR with $\Delta x = 0.01$ cm (dotted), UDE on the same grid (grey), and WARK on the same grid (dashed). Bottom row: corresponding plots of local D_f (left) and CWT spectrum (right) vs. scale.

Acknowledgements

This work is available as Los Alamos National Laboratory report LA-UR-02-2212, and was performed at Los Alamos National Laboratory, which is operated by the University of California for the United States Department of Energy under contract W-7405-ENG-36.

References

[1] R. M. Baltrusaitis, M. L. Gittings, R. P. Weaver, R. F. Benjamin, J. M. Budzinski, *Simulation of Shock Generated Instabilities*, Phys. Fluids, 8, (1996), 2471–2493.

[2] J. Bell, M. Berger, J. Saltzman, M. Welcome, *3-Dimensional Adaptive Mesh Refinement for Hyperbolic Conservation Laws*, SIAM J. Sci. Comput., 15, (1994), 127–138.

[3] M. Brouillette, *The Richtmyer-Meshkov Instability*, Annual Rev. Fluid Mech., 34, (2002), 445–468.

[4] P. E. Dimotakis, H. J. Catrakis, A. W. Cook, J. M. Patton, *On the geometry of two-dimensional slices of irregular level sets in turbulent flows*, GALCIT report FM98-2, available at `http://www.its.caltech.edu/%7Epxdgroup/pub/98/dimotakis_ccp.98a.pdf`.

[5] B. Dubuc, S. W. Zucker, C. Tricot, J. F. Quiniou, D. Wehbi, *Evaluating the fractal dimension of surfaces*, Proc. Roy. Soc. Lond. A, 425, (1989), 113–127.

[6] M. Farge, *Wavelet Transforms and Their Applications to Turbulence*, Ann. Rev. Fluid Mech., 24, (1992), 395–457.

[7] G. Gonzato, *A Practical Implementation of the Box Counting Algorithm*, Computers & Geosciences, 24, (1998), 85–100.

[8] Q. Huang, J. R. Lorch, R. C. Dubes, *Can the Fractal Dimension of Images be Measured?*, Pattern Recognition, 27, (1994), 339–349.

[9] J. R. Kamm, W. J. Rider, P. M. Rightley, K. P. Prestridge, R. F. Benjamin, P. Vorobieff, *The gas curtain experimental technique and analysis methodologies*, in Y. Villacampa Esteve, G. M. Carlomagno, C. A. Brebbia, eds., *Proceedings of the Tenth International Conference on Computational Methods and Experimental Measurements, Alicante, 2001*, WIT Press, Southampton (2001), pp. 85–94.

[10] J. Lewalle, *Three Lectures on the Application of Wavelets to Experimental Data Analysis*, VKI Lecture Series Notes 1998, available at `ftp.mame.syr.edu` in subdirectory `/pub/jlewalle`.

[11] K. P. Prestridge, P. Vorobieff, P. M. Rightley, R. F. Benjamin, *Validation of an instability growth model using particle image velocimetry measurements*, Phys. Rev. Lett., 84, (2000), 4353–4356.

[12] W. J. Rider, *An Adaptive Riemann Solver Using a Two-Shock Approximation*, Comp. Fluids, 28, (1999), 741–777.

[13] W. J. Rider, J. R. Kamm, P. M. Rightley, K. P. Prestridge, R. F. Benjamin, P. Vorobieff, *Direct statistical comparison of hydrodynamic mixing experiments and simulations*, in Y. Villacampa Esteve, G. M. Carlomagno, C. A. Brebbia, eds., *Proceedings of the Tenth International Conference on Computational Methods and Experimental Measurements, Alicante, 2001*, WIT Press, Southampton (2001), pp. 199–208.

[14] W. J. Rider, J. R. Kamm, C. A. Zoldi, *How do numerical methods effect the statistical details of Richtmyer-Meshkov instabilities?*, in F. Lu, ed., *Proceedings of the 23rd International Symposium on Shock Waves, Fort Worth, 2001*, to appear (2002).

[15] W. Rider, L. Margolin, J. Kamm, *An Adaptive Time Integration Algorithm for Hyperbolic Conservation Laws*, in T. Hou, E. Tadmor, eds., *Proceedings of the Ninth International Conference on Hyperbolic Problems, Pasadena, 2002*, to appear (2002).

[16] P. M. Rightley, P. Vorobieff, R. F. Benjamin, *Evolution of a Shock Accelerated Thin Fluid Layer*, Phys. Fluids, 9, (1997), 1770–1783.

[17] P. M. Rightley, P. Vorobieff, R. Martin, R. F. Benjamin, *Experimental-Observations of the Mixing Transition in a Shock-Accelerated Gas Curtain*, Phys. Fluids, 11, (1999), 186–200.

[18] K. R. Sreenivasan, *Fractals and Multifractals in Fluid Turbulence*, Ann. Rev. Fluid Mech., 23, (1991), 539–600.

[19] C. Tomkins, K. P. Prestridge, P. M. Rightley, P. Vorobieff, R. F. Benjamin, *Flow morphologies of two shock-accelerated, unstable gas cylinders*, J. Visualization, to appear (2002).

[20] G. Treviño, E. L. Andreas, *On Wavelet Analysis of Nonstationary Turbulence*, Boundary-Layer Meteorology, 81, (1996), 271–288.